Thieno, Furo, and Selenopheno[3,4-c]pyrrole-4,6-dione Copolymers: Air-Processed Polymer Solar Cells with Power Conversion Efficiency up to 7.1%

ARTICLE *in* ADVANCED ENERGY MATERIALS · SEPTEMBER 2015

Impact Factor: 16.15 · DOI: 10.1002/aenm.201501213

9 AUTHORS, INCLUDING:

Nicolas Allard

Laval University

7 PUBLICATIONS **181** CITATIONS

SEE PROFILE

Mariane Ouattara

Laval University

2 PUBLICATIONS **5** CITATIONS

SEE PROFILE

Mario Leclerc

Laval University

223 PUBLICATIONS **18,477** CITATIONS

SEE PROFILE

ADVANCED ENERGY MATERIALS
www.advenergymat.de

Thieno, Furo, and Selenopheno[3,4-*c*]pyrrole-4,6-dione Copolymers: Air-Processed Polymer Solar Cells with Power Conversion Efficiency up to 7.1%

*Ahmed Najari, Serge Beaupré, Nicolas Allard, Mariane Ouattara, Jean-Rémi Pouliot, Patrick Charest, Simon Besner, Martin Simoneau, and Mario Leclerc**

Polymers based on thieno[3,4-*c*]pyrrole-4,6-dione derivatives are interesting and promising candidates for organic bulk heterojunction solar cells. Herein, a series of push–pull conjugated polymers based on thieno[3,4-*c*]pyrrole-4,6-dione (TPD), furo[3,4-*c*]pyrrole-4,6-dione (FPD), and selenopheno[3,4-*c*]-pyrrole-4,6-dione (SePD) have been synthesized by direct heteroarylation polymerization and fully characterized. The impacts of both the heteroatom (sulfur, oxygen, and selenium) and the side chain (branched or linear) of [3,4-*c*]pyrrole-4,6-dione unit on the electro-optical properties have been investigated. Among polymers developed, two new highly processable terthiophene–SePD (P4) and dithienosilole–SePD (P9) copolymers led to air-processed polymer solar cells with power conversion efficiencies of 5.1% and 7.1% using the following inverted configuration: ITO/ZnO/Polymer:PCBM/MoO_3/Ag. These promising results make P4 and P9 good candidates for further upscaling and device optimization.

1. Introduction

Light-weight, flexibility, low-cost, and easy fabrication are key words when one refers to bulk heterojunction (BHJ) plastic solar cells (PSCs). Due to all these potential advantages, this technology has received great attention in the last two decades. For instance, state-of-the-art organic solar cells based on small molecules now reach power conversion efficiencies (PCEs) of >9%.[1–5] whereas polymer-based organic solar cells have achieved power conversion efficiencies of >10%.[6] Moreover, some polymeric solar cells have exhibited lifetimes up to 7–10 years.[7–11] This progress of the efficiency of polymer-based BHJ solar cells is partly related to the development of new, well-designed, high molecular weight, and processable materials.[12–14] Very recently, Liu et al. and Heeger and co-workers achieved PCEs of 10.8% and 9.4%, respectively, with impressive short current densities (J_{sc}) of 18.8 and 20.07 mA cm^{-2} for thick films (thickness up to 300 nm).[7,15] Along these lines, thieno[3,4-*c*]pyrrole-4,6-dione (TPD)-based copolymers are among the most efficient donors in BHJ organic solar cells.[16–20] Indeed, some TPD-based PSCs have exhibited PCEs up to 8.5% when fabricated and tested under inert atmosphere.[17–21] Among them, a new terthiophene–TPD copolymer (**P1**) prepared by new and innovative direct heteroarylation polymerization (DHAP) led to PCE >6.0% with an open-circuit voltage (V_{oc}) up to 0.94 V in single-junction classical configuration.[22] Heterocyclic[3,4-*c*]pyrrole-4,6-dione as electron acceptor moieties allows interesting advantages for plastic electronics and especially for photovoltaic applications: fine tuning of the highest occupied molecular orbital (HOMO) and lowest unoccupied molecular orbital (LUMO) energy levels, solubility, and crystallinity via imide *n*-alkylation, coplanarity, and high molecular weights.[23] On the basis of these promising results, we have reported a series of light-absorbing conjugated copolymers based on [3,4-*c*]pyrrole-4,6-dione derivatives.[24] As a follow-up of our previous work, we prepared "push–pull" conjugated polymers based on furo[3,4-*c*]pyrrole-4,6-dione (FPD), selenopheno[3,4-*c*]pyrrole-4,6-dione (SePD), and TPD in order to investigate the effects of the heteroatom and the alkyl chain on the photovoltaic performance. More importantly, all devices have been fabricated and characterized in air using the inverted configuration, which can lead to simple and low-cost manufacturing processes.

Dr. A. Najari, Dr. S. Beaupré, Dr. N. Allard, M. Ouattara, J.-R. Pouliot, Prof. M. Leclerc
Canada Research Chair on Electroactive and Photoactive Polymers
Department of Chemistry
Université Laval
Quebec City, Quebec G1V 0A6, Canada
E-mail: Mario.Leclerc@chm.ulaval.ca
P. Charest, Dr. S. Besner, Dr. M. Simoneau
Institut de recherche d'Hydro-Québec (IREQ)
Varennes, Quebec J3X 1S1, Canada

DOI: 10.1002/aenm.201501213

2. Results and Discussion

With the exception of polymer **P9** which was prepared from standard Stille coupling, all copolymers were synthesized using DHAP between dibrominated terthiophene derivatives and pyrrole-dione moieties (**Figure 1**). All synthetic details are reported in the Experimental Section. Molecular weights

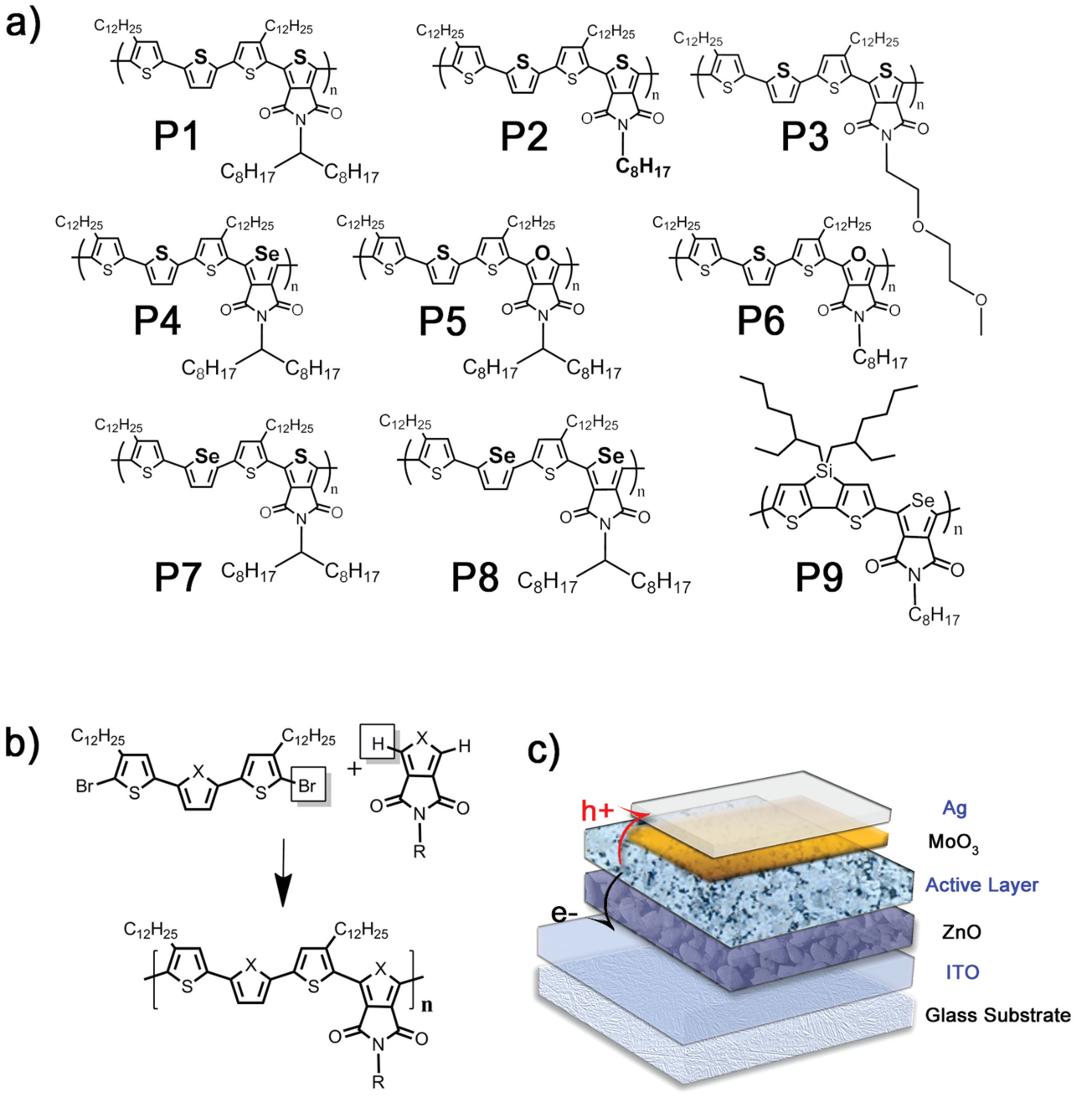

Figure 1. a) Chemical structure of the investigated push–pull copolymers. b) Synthetic steps and molecular structure of terthiophene core and halogeno[3,4-*c*]pyrrole-4,6-dione derivatives, and c) schematic of BHJ polymer solar cells.

were measured by size-exclusion chromatography in hot 1,2,4-trichlorobenzene (110 °C) using monodisperse polystyrene standards. Thermogravimetric analyses revealed that all polymers are stable up to 400 °C (Figure S1, Supporting Information).

As mentioned above, copolymer (**P1**) was already studied by Heeger and co-worker using [6,6]-phenyl C71-butyric acid methyl ester [70]PCBM as an electron acceptor and 1-chloronaphthalene as an additive. [22] It has been shown that polymer (**P1**) presented a mobility of 0.013 $cm^2\ V^{-1}\ s^{-1}$ and a PCE of about 6.0% in a conventional configuration.

In this work, **P2** and **P3** have been synthesized in the same polymerization conditions used for **P1** in order to investigate the influence of the side chain in the TPD unit on the electro-optical properties, the morphology of the BHJ, and the photovoltaic behaviour (**Figure 2**). As shown in **Table 1** and Figure 2a, the optical band gap (E_g^{opt}) for **P2** and **P3** (1.87 and 1.80 eV, respectively) is similar to **P1** (≈1.81 eV). Moreover, the electrochemical band gaps (E_g^{cv}) of **P1** (1.80 eV), **P2** (1.83 eV), and **P3** (1.77 eV) estimated from the difference between the onset potentials for oxidation and reduction (from cyclic voltammetry measurements) are in a good agreement with those obtained

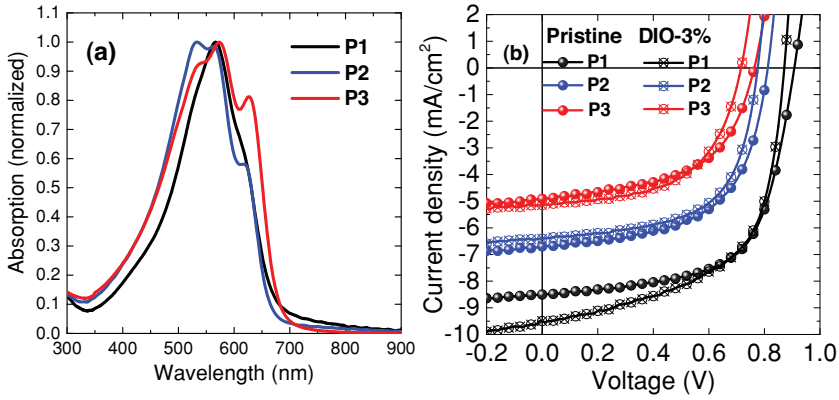

Figure 2. a) Normalized UV–vis absorption spectra of films of polymers **P1**, **P2**, and **P3**. b) *J–V* curves of inverted solar cells of polymers **P1**, **P2**, and **P3**:[60]PCBM.

from UV–vis spectra (E_g^{opt}). Figure 2b represents the typical *J–V*) curves of polymers **P1–P3**. Since our work is also focused on the development of reliable processing methods which can lead to low-cost, stable, and large-scale polymeric solar cells, all devices were fabricated and tested in air with the following inverted configuration: ITO/ZnO/Polymer: [6,6]-phenyl-C61 butyric acid methyl ester ([60]PCBM) or [70]PCBM/MoO_3/Ag. The active area of each cell was 0.24 cm^2 and the current density–voltage (*J–V*) measurement was carried out under simulated AM1.5 solar illumination (100 mW cm^{-2}).

Inverted organic photovoltaics (OPV) configuration combines enhanced stability and large-scale processability when compared to conventional architecture devices using poly(3,4-ethylenedioxythiophene):polystyrene sulphonate (PEDOT:PSS) as hole transporting layer. [21,25,26] Indeed, the stability of layered structures is an important parameter for the viability of polymeric-based devices. Degradation mechanisms are still under investigation but several processes have already been identified such as detrimental diffusion of indium atoms (from indium tin oxide (ITO) layer) in the bulk heterojunction, oxidation of the active layer under ambient conditions, and PEDOT:PSS interactions with the BHJ.[27] These degradation mechanisms can have important effects on the efficiency of polymeric solar cells. Indeed, Cao and co-workers have reported a dramatic drop of the PCE for PTB7 when comparing conventional and inverted structures. Indeed, a decrease of more than 80% (within 20 d) was observed for devices using the conventional structures. On the other hand, inverted devices retained more than 95% to their initial performances after 60 d.[25]

Upon side chain modification on the TPD unit (**P1** to **P3**), the best performance was obtained for polymer **P1** with a PCE of up to 4.96%, a short-circuit current (J_{sc}) of 9.50 mA cm^{-2}, an open circuit voltage (V_{oc}) of 0.87 V, and a fill factor (FF) of 0.60 (**Table 2**). The difference of PCE for these polymers could be partly explained by a variation of the V_{oc} directly linked to the HOMO energy level, tuned by the side chain on the TPD core. Indeed, the V_{oc} values (Table 2) decrease from 0.91 to 0.76 V without additives and from 0.87 to 0.72 V by using diiodooctane (DIO) for **P1** to **P3**, respectively.

According to the literature, sulfur, oxygen, and selenium heteroatom in the heterocycle may also have an impact on intermolecular interactions, planarity, solubility, molecular weight, and, thus, on energy levels and optical properties.[24,27] To continue our investigation on these promising copolymers, the heteroatom in the TPD core (with branched and straight alkyl side chains) was also changed. As reported in Tables 1 and 2, our strategy was effective, and significant effects of the heteroatoms on the electro-optical and photovoltaic properties have been observed.

As observed in **Figure 3**, polymers **P1**, **P2**, **P4**, **P5**, and **P6** show a broad UV–vis absorption spectrum, with an optical band gap (E_g^{opt}) ranging from 1.79 to 1.93 eV. The electronic band gap values E_g^{cv} (Table 1) are in a relatively good correlation with E_g^{opt}. Interestingly, thin film UV–vis absorption spectra of polymers **P1**, **P4**, and **P5** indicate a hypsochromic shift of the optical band gap for FPD and a bathochromic shift for SePD compared to

Table 1. Molecular weights, and optical and electrochemical properties of copolymers **P1** to **P9**. The bold values are the absorption maxima.

Polymer	$\bar{M}_n$ [kDal]	$\bar{M}_w$ [kDal]	PDI	T_d [°C]	Film l_{max} [nm]	E_{HOMO}/E_{LUMO} [eV]/[eV]	E_g^{cv} [eV]	E_g^{opt} [eV]
P1	44	110	2.5	434	**567**–617(s)[a)]	–5.66/–3.86	1.80	1.81
P2	27	52	1.9	427	**534**–**565**–615(s)	–5.56/–3.73	1.83	1.87
P3	11	20	1.8	421	540(s)–**573**–627(s)	–5.31/–3.54	1.77	1.80
P4	42	81	1.9	416	**590**–645(s)	–5.57/–3.69	1.88	1.79
P5	20	55	2.7	422	**545**–590(s)	–5.65/–3.80	1.85	1.93
P6	41	70	1.7	424	**563**–608(s)	–5.54/–3.75	1.79	1.87
P7	36	71	2.0	437	593–639(s)	–5.49/–3.82	1.67	1.78
P8	41	85	2.1	422	**578**	–5.48/–3.69	1.79	1.76
P9	29	45	1.6	442	447(s)–**365**–**697**	–5.55/–3.82	1.73	1.68
PDTSTPD	28	44	1.6	–	445–620–**680**	–5.57/–3.88	1.69	1.73[20]

[a)]Shoulder.

Table 2. Device characteristics of OPV devices with and without DIO-3% v/v from conjugated copolymers based on furo, selenopheno, and thieno[3,4-*c*]pyrrole-4,6-dione derivatives blended with [60]PCBM or [70]PCBM.

Polymer	Thickness [nm]	DIO [v/v]	J_{sc} [mA cm^{-2}]	V_{oc} [V]	FF	PCE [%]	PCE [% average]	R_{sh} [kΩ cm^{-2}]	R_s [Ω cm^{-2}]
P1	80–90	0%	8.50	0.91	0.63	4.87	4.78 ± 0.10	2.4	22
		3%	9.50	0.87	0.60	4.96	4.84 ± 0.05	0.7	12
P2	70–80	0%	6.70	0.81	0.59	3.20	2.92 ± 0.11	1.3	19
		3%	6.41	0.78	0.61	3.05	2.81 ± 0.25	1.8	17
P3	70–80	0%	4.91	0.76	0.56	2.09	1.99 ± 0.09	1.3	34
		3%	5.14	0.72	0.56	2.07	1.93 ± 0.18	2.4	30
P4	80–90	0%	4.93	0.95	0.49	2.29	1.79 ± 0.13	0.9	35
		3%	8.80	0.88	0.66	5.11	5.01 ± 0.15	1.6	13
P5	70–80	0%	1.06	0.86	0.36	0.33	0.30 ± 0.04	1.3	240
		3%	1.57	0.81	0.39	0.50	0.43 ± 0.10	2.5	770
P6	75–85	0%	6.66	0.81	0.62	3.34	3.16 ± 0.19	2.3	21
		3%	6.76	0.80	0.63	3.40	3.26 ± 0.15	2.0	17
P7	80–90	0%	8.14	0.88	0.61	4.37	4.28 ± 0.11	1.0	15
		3%	6.64	0.89	0.55	3.25	3.00 ± 0.14	1.5	25
P8	85–100	0%	5.61	0.93	0.45	2.35	2.13 ± 0.12	0.6	28
		3%	7.75	0.87	0.68	4.59	4.41 ± 0.19	1.6	9
P9 ([60]PCBM)	85–90	0%	5.48	0.88	0.56	2.70	2.64 ± 0.05	0.6	13
		3%	10.40	0.85	0.63	5.60	5.54 ± 0.08	0.9	7
P9 ([70]PCBM)	70–85	3%	13.17	0.85	0.64	7.13	7.03 ± 0.08	0.5	5

TPD (Figure 3a). This behavior was, however, not observed for polymers **P2** and **P6** (TDP and FDP with a straight octyl side chain linked in the nitrogen atom) (Figure 3b). This could be related to the lower molecular weights of **P5** compared to **P1** and **P4**. Indeed, despite several attempts, the highest number-average molecular weight obtained for **P5** was of 20 kDa with a polydispersity index of 2.7. Those values are much lower than those obtained for **P1** and **P4** (M_n = 44 kDa, PDI = 2.5; M_n = 42 kDa, PDI = 1.9, respectively). Moreover, as shown in **Figure 4**, photovoltaic properties of polymers **P1**, **P2**, **P4**, **P5**, and **P6** are clearly influenced by the chemical structure of the electron-poor unit of the polymers. Indeed, a significant drop of the PCE (curves without DIO) was observed for TPD, FPD, and SePD comonomers bearing a branched alkyl side chain (Figure 4a). In fact, **P4** and **P5** reached PCEs of 2.29% and 0.36% (≈4.90% for **P1**), J_{sc} of 4.93 and 1.06 mA cm^{-2}, FF of 0.49 and 0.36, and V_{oc} of 0.95 V and 0.86 V, respectively (see Table 2). However, by using DIO as an additive in BHJ, the power conversion efficiency of **P4** increases significantly unlike **P5**. In fact, with a weight ratio of 1:1.5 for **P4**: [60]PCBM, the best device exhibits a PCE of 5.11%, a J_{sc} of 8.80 mA cm^{-2}, an interesting FF of 0.66, and a V_{oc} of 0.88 V.

Additives as DIO are known to be favorable for charge transport by dissolving the donor and the acceptor into the active solution and thus enabling a better interpenetration of both materials in the BHJ after thin film deposition.[28–31] Nevertheless, although the J_{sc} is enhanced from 4.93 to 8.80 mA cm^{-2}, the V_{oc} is decreased from 0.95 to 0.88 V (dropping observed with the majority of polymers studied in this work). In the case of **P5**, the shunt resistance (R_{sh}) is high and the *J*–*V* curve shows an S shape (for DIO-3% only). According to the literature, this kind of behavior can be related to charge accumulation between the active layer and the electrode.[32] The high optical density and the broad absorption of **P4** compared to **P1** and **P5** (Figure S3, Supporting Information) highlight a strong potential of the SePD as a candidate for plastic solar cells.

These photovoltaic results could also be partially explained by the nanomorphology in the BHJ. Indeed, as observed in **Figure 5**, the

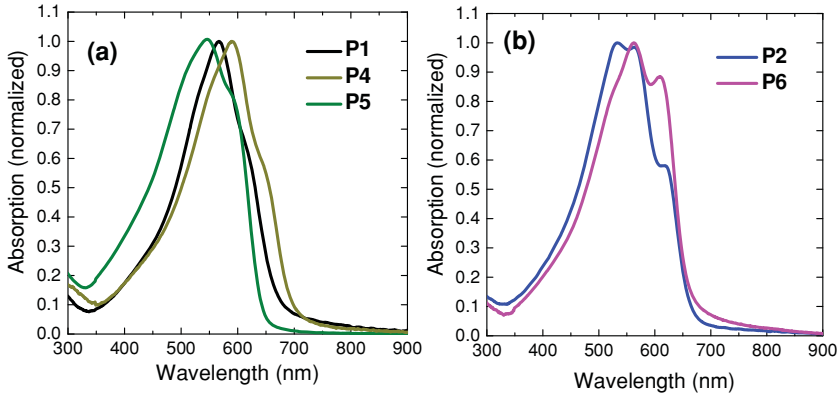

Figure 3. a) Normalized UV–vis absorption spectra of films of polymers **P1**, **P4**, and **P5**. b) Normalized UV–vis absorption spectra of films of polymers of **P2** and **P6**.

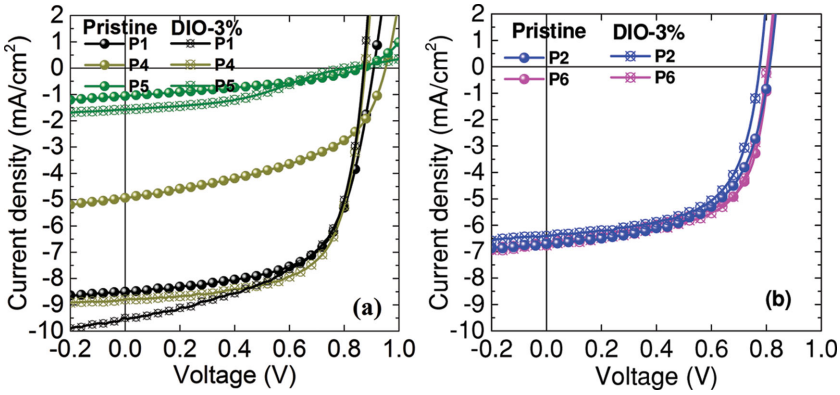

Figure 4. *J–V* curves of polymers:[60]PCBM BHJ (with and without DIO-3% v/v) solar cells. a) Impact of the heteroatom on the pyrrole-dione unit (**P1**, **P4**, and **P5**). b) Effect of side chain on TPD versus FPD (**P2** and **P6**).

atomic force microscopic (AFM) topography images (height and phases) of polymers, [60]PCBM blend films (1:1.5 w/w), clearly show a different topology for **P1**, **P4**, and **P5**. For these last polymers, AFM images show large domains (over 100 nm) which imply a lower J_{sc} caused by the reduction of interface between the donor and the acceptor. Nevertheless, it is clear that the nanomorphology for **P4** is modified by using DIO, showing a continuous interpenetrating network while the morphology of **P5** remains unchanged. As reported in the literature, the additives significantly increase surface root-mean-square (RMS) roughness, as observed for all polymers: [60, 70]PCBM (**P1** to **P9**; see Figure 5 and the Supporting Information) excepted for **P5**.[33,34] Those results indicate that the BHJ films with processing additives of DIO allow a better nanomorphology between donors and acceptors by removing aggregated regions. The RMS roughness of **P5**:fullerene blend decreases from 2.0 to 1.5 nm with and without DIO, respectively, and as shown in AFM phase image (Figure 5), the film presents a large separated morphology with no indication of bicontinuous networks. Moreover, low molecular weight of **P5** has to be considered as an important factor that limits the overall performance of this material since electro-optical properties are known to be molecular weight dependent.

As shown in Figure 5, unlike **P5**, the morphology of polymers **P2** and **P6** is comparable to **P1** in terms of phase separation. Indeed, the AFM images show the formation of a good nanoscale separation between the polymeric donor and the [60]PCBM acceptor, which is the key for efficient charge generation and transport. **P2** and **P6** show interesting polymers' photovoltaic behavior in inverted solar cells with PCEs of 3.20% and 3.34% and FF of 0.59 and 0.62, respectively (Figure 4b and Table 2).

To learn more about the effect of the selenium atom on terthiophene and pyrrolodione core and their impact on the electro-optical and photovoltaic properties, **P1**, **P4**, **P7**, and **P8** have been compared. As shown in **Figure 6**a, polymers **P1** and **P7** exhibit a broad UV–vis absorption spectrum with an optical band gap of 1.81 and 1.78 eV, respectively. A slight bathochromic shift of the absorption spectrum of **P7** combined with a higher HOMO energy (–5.49 vs –5.66 eV) clearly shows the effect of the selenophene on the electro-optical properties.

As reported in the literature, the photocurrent and thus the performance of **P7** decrease strongly with the addition of additives into the BHJ (Figure 6b, Table 2).[35] The PCEs of **P1** and **P7** without DIO are 4.87% and 4.37%, respectively. In those conditions, despite better solubility of **P7** compared to **P1**, it is clear that the substitution of a central thiophene (**P1**) by a selenophene (**P7**) on the terthiophene unit linked to a TPD core was not beneficial for the overall performance. The same conclusion can be drawn for the results obtained for **P4** versus **P8**: limited effects on the electro-optical properties and lower PCE for **P8** versus **P4** (see **Figure 7** and Table 2). On the other hand, the replacement of TPD (**P1**) by SePD (**P4**) led to PCE up to 5.11% compared to 4.96% for **P1**. According to Table 1, the use of SePD (**P4**) has a slight effect on both the HOMO energy level (–5.57 vs –5.66 eV) and the optical band gap (1.79 vs 1.81 eV) when compared to **P1**. Since the processability of the polymer is a key point for polymeric solar cells, we noticed that **P4** was more soluble than **P1**. While **P1** has to be processed from hot solutions, **P4** was readily soluble at room temperature. This advantage can lead to a better control and reproducibility of the deposition of the BHJ active layer by usual casting methods. AFM images show the formation of a good nanoscale separation for both **P1** and **P4**, and [60]PCBM (Figure 5), but excepting the RMS values between **P1** (1.6 nm) and **P4** (2.2 nm), nanomorphologies seem to be relatively similar.

Based on these results, the SePD comonomer seems to have a positive impact on the electro-optical properties and on the solubility of the resulting polymers which led to enhanced photovoltaic performance. Since TPD-based copolymers are known to yield highly performing polymeric solar cells, we have prepared a new polymer (**P9)** based on dithienosilole and SePD using Stille cross-coupling reaction (Figure 1).[36,37] This polymerization has been optimized for the synthesis of **P9** since it led to molecular weights comparable to those obtained for PDTSTPD, a highly efficient TPD-based material. Recently, PDTSTPD was synthesized by direct heteroarylation polymerization but only low molecular weights were obtained. More importantly, DHAP led to insoluble materials and broad molecular weight distribution.[38,39] For those reasons, we did utilize the DHAP method for the synthesis of **P9**.

As mentioned above, polymer **P9** is an analog of PDTSTPD, a polymer already reported in the literature.[37,40] As for terthiophene–pyrrole-dione derivatives, the use of SePD instead of TPD slightly modified the optical properties. Indeed, the E_g^{opt} of **P9** (1.68 eV) is 0.05 eV lower than the optical band gap of PDTSTPD (E_g^{opt} = 1.73 eV). The HOMO and LUMO energy levels were slightly modified, thus keeping a high open circuit voltage around 0.85–0.88 V. As shown in Table 2 and **Figure 8**b, the best photovoltaic performance of **P9** was obtained by using [70]PCBM as an acceptor and DIO-3% v/v as an additive with a V_{oc} of 0.85 V, a J_{sc} of 13.17 mA cm^{-2}, an FF of 0.64, and an interesting PCE of 7.13%. In the same configuration (ITO/ZnO/polymer: [70]PCBM/MoO_3/Ag), Chu et al.[36] achieved for PDTSTPD a PCE of 6.6%, a V_{oc} of 0.88 V, a J_{sc} of 10.50 mA cm^{-2},

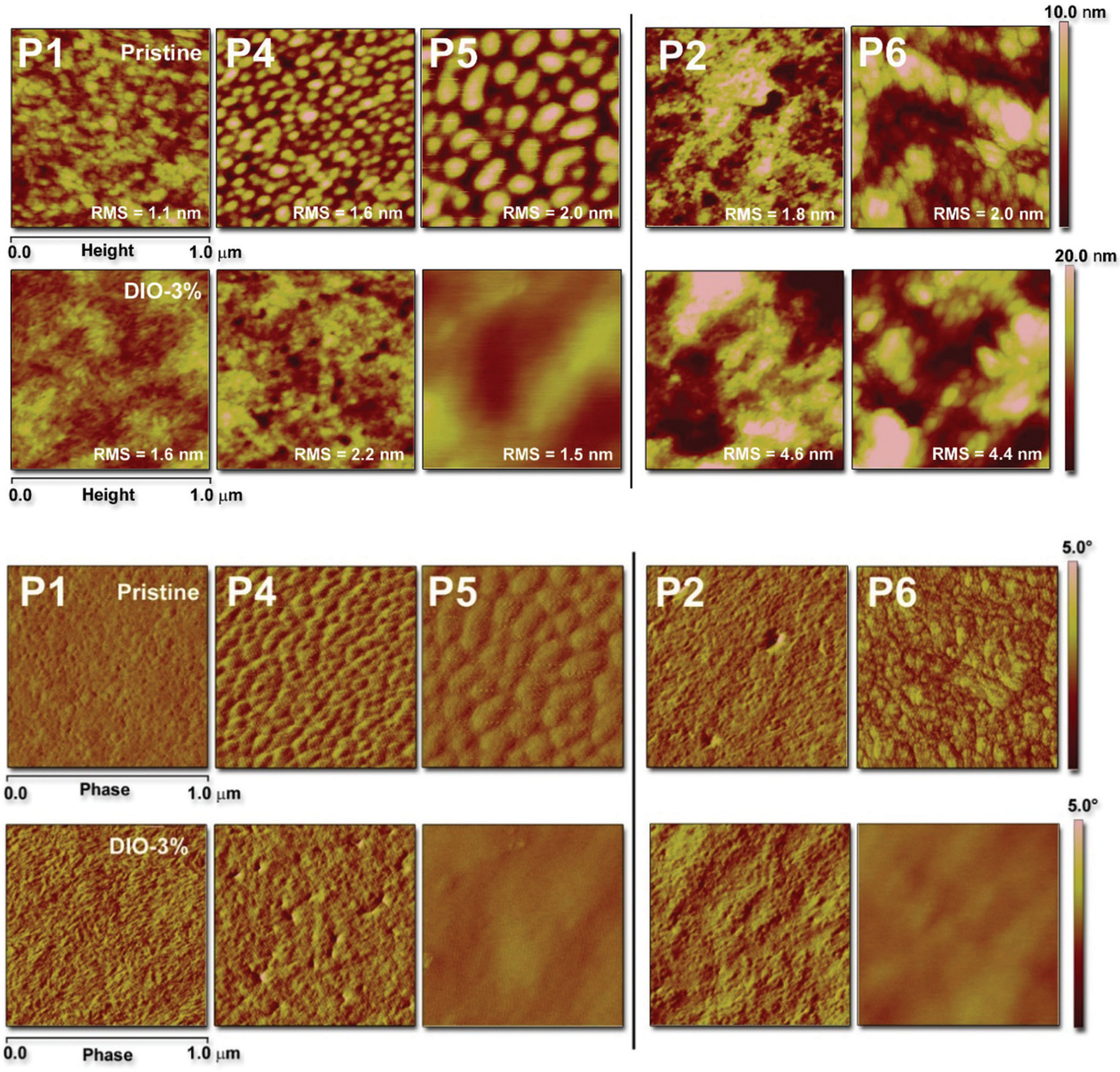

Figure 5. AFM image topography (height and phase) of polymers **P1**, **P2**, **P4**, **P5,** and **P6**:[60]PCBM blend films (1:1.5 w/w) with and without DIO-3% v/v processed from *ortho*-dichlorobenzene.

and an FF of 0.71. A mobility ranged between 1×10^{-4} and 4×10^{-4} cm^2 V^{-1} s^{-1}, and a PCE of 7.50% were achieved in a conventional configuration.[37,40]

High efficiency of **P9** blended with [60]PCBM or [70]PCBM could be explained in part by the nanomorphology of **P9**:PCBM blend as shown in **Figure 9**. Indeed, in the case of the active layer obtained without additives, one can see large and isolated domains (more than 250 nm). Upon addition of DIO, better percolation was obtained which can contribute to a better and most efficient charge transport. It is worth noting that all the experiments were done in air, which means that a PCE of 7.13% is among the highest value reported so far for such a kind of experimental setup.

3. Conclusion

Inverted polymer solar cells using push–pull conjugated polymers based on FPD, SePD, and TPD derivatives and terthiophene moieties were prepared from direct (hetero)arylation and fully characterized. These studies have revealed that SePD-based copolymers can exhibit very promising photovoltaic properties. These observations led us to synthesize and characterize a new polymer (**P9**) with a high power conversion efficiency of 7.13% in air. Finally, in terms of manufacturing, the next step would be a process that involves only printing steps and would therefore avoid the evaporation of the MoO_3 and Ag layers. All these challenges are currently investigated.

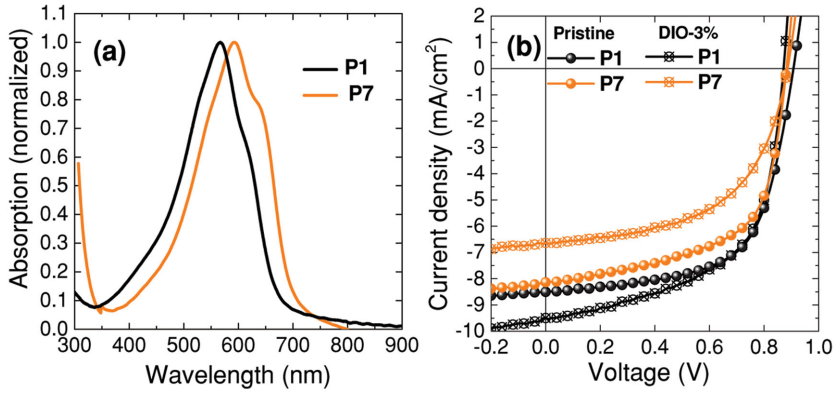

Figure 6. a) Normalized UV–vis absorption spectra of films of **P1** and **P7**. b) *J–V* curves of inverted solar cells of **P1** and **P7**.

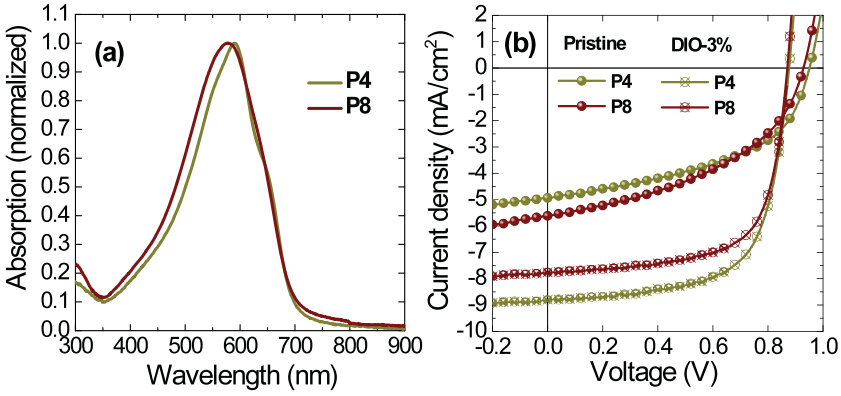

Figure 7. a) Normalized UV–vis absorption spectra of films of **P4** and **P8**. b) *J–V* curves of inverted solar cells of **P4** and **P8**.

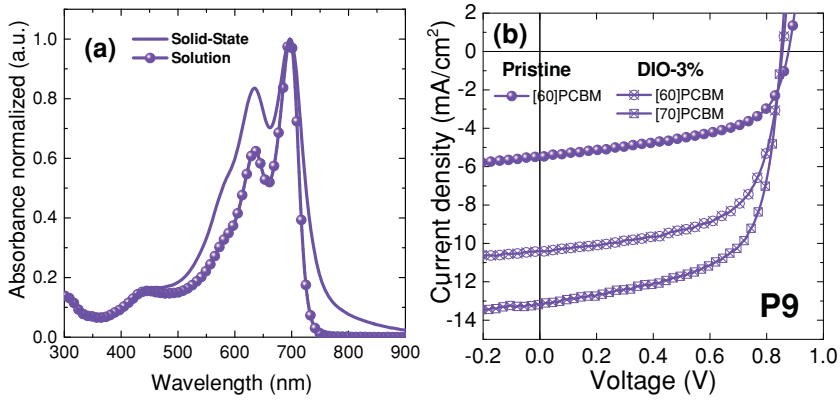

Figure 8. a) Normalized UV–vis absorption spectra and external quantum efficiency (EQE) of **P9** with DIO-3%. b) *J–V* curves of inverted solar cells of **P9**.

4. Experimental Section

Characterization: Cyclic voltammograms were recorded on a Solartron 1287 potentiostat using platinum wires as working electrode and counter-electrode at a scan rate of 50 mV s^{-1}. The reference electrode was Ag/Ag^+ (0.01 M of $AgNO_3$ in acetonitrile) and the electrolyte was a solution of 0.1 M of tetrabutylammonium tetrafluoborate in dry acetonitrile. In these conditions, the oxidation potential of Ferrocene was 0.09 V versus Ag/Ag+, whereas the oxidation potential of Ferrocene was 0.41 V versus saturated calomel electrode (SCE). The HOMO and LUMO energy levels were determined from the oxidation and reduction onsets (where the current differs from the baseline) assuming that SCE electrode is –4.7 eV from vacuum, as reported in the literature.[41] AFM images were obtained using a Veeco's Dimension V AFM in the tapping mode.

Fabrication and Characterization of Inverted Solar Cell Devices: The inverted BHJ solar cells were prepared on commercial ITO-coated glass substrate (24 × 24 mm) with a sheet resistance of 10 Ω $square^{-1}$ (Thin Film Devices Inc, USA). The thickness of ITO layer is about 250 nm. Each substrate was patterned using photolithography techniques to produce a segment with active areas of 24 mm^2. The substrates were sonicated sequentially in cleanroom detergent, deionized (DI) water, acetone, and isopropyl alcohol. Immediately prior to devices fabrication, the substrates were treated in a plasma–oxygen chamber (Spacemaker II sensor, Plasmatic Systems, Inc, USA) for 5 min. First, a ZnO thin film of about 40 nm was filtered through a 0.45 µm poly(tetrafluoroethylene) (PTFE) filter and spin-cast on top of the ITO electrode. The preparation of the ZnO precursor was performed according the synthesis described by Heeger and co-workers.[42] Thereafter, the ZnO film was baked at 200 °C for 60 min in the air. Bulk heterojunction photoactive layers were filtered through a 0.45 µm PTFE filter and deposited onto the ZnO layer by spin-coating with blend solutions composed of polymer and [60]PCBM from Nano-C, USA. All the blend solutions were prepared by dissolving the polymers (10 mg mL^{-1}) and [60]PCBM (15 mg mL^{-1}) in 1,2-dichlorobenzene solvent and stirred on the hotplate at room temperature overnight in the air. After the photoactive layers deposition, the substrates were dried at room temperature in the air. Layer thicknesses (70–100 nm) were measured using a Veeco Deltak IIA surface profiler. Finally, MoO_3 (8 nm) and Ag (100 nm) were sequentially vacuum-deposited under a shadow mask on top of the active layer by thermal evaporation under high vacuum (2 × 10^{-5} Torr). Current versus potential curves (*J–V* characteristics) were measured with a Keithley 2400 Digital Source Meter under a collimated beam. Illumination of the cells was done through the ITO side using light from 150 W Oriel Instruments Solar Simulator and a xenon lamp with an AM1.5G filter to provide an intensity of 100 mW cm^{-2} calibrated with a KG-5 filtered silicon photodiode. Device optimization involved over 400 devices made from over 100 substrates prepared polymers:[60 or 70]PCBM films. All device fabrications and characterizations were performed in an ambient environment without any protective atmosphere and without any encapsulation.

Materials. Synthesis of Monomers and Polymers: TPD-based copolymers **P1**, **P2**, **P3**, and **P7** and FPD-based copolymers **P5** and **P6** were prepared according to the literature.[22,24,35,37,43] Synthesis of 1,3-dibromo-5-octyl-4H-selenopheno[3,4-*c*]pyrrole-4,6(5H)-dione (dibromoSePD) and 4,4-bis(2-ethylhexyl)-2,6-bis(trimethyltin)-dithieno[3,2-*b*:2′,3′-*d*]silole

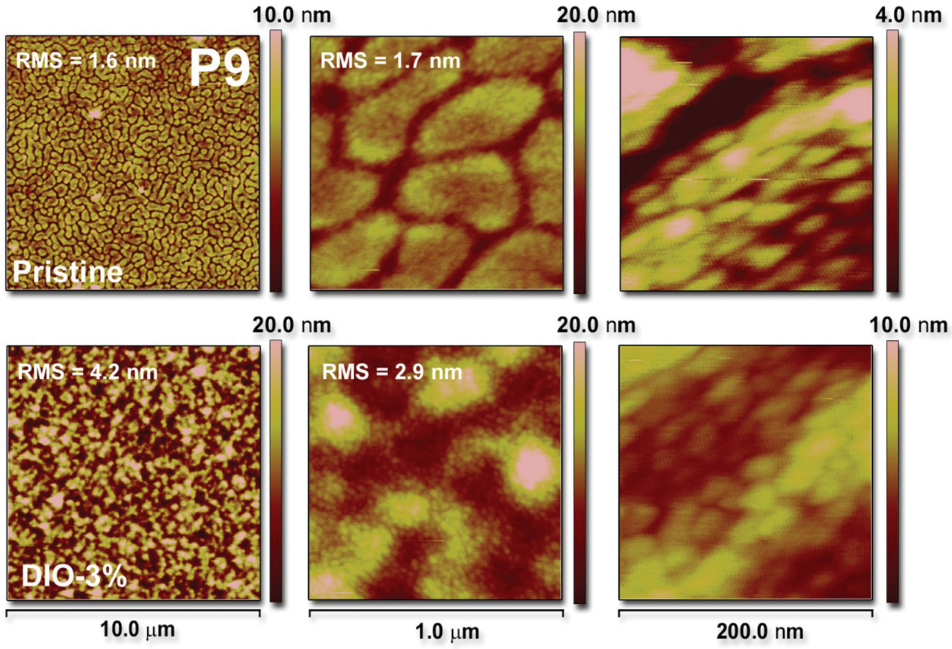

Figure 9. AFM topography (height) of **P9**:[60]PCBM blend films (1:2 w/w) with and without DIO-3% v/v processed from chloroform.

was carried out according to the following literature in order to obtain polymer **P9** by the Stille cross-coupling reaction. [16]

*Polymer **P4** Synthesis*: 5,5″-dibromo-4,4″-didodecyl-2,2′:5″,2″-terthiophene (0.0743 g, 0.1 mmol), 5-(9-heptadecanyl)selenopheno[3,4-*c*]pyrrole-4,6-dione (0.0439 g, 0.1 mmol), palladium (II) acetate (1.12 mg, 5% mol), pivalic acid (10.2 mg, 0.1 mmol), tris(2-methoxyphenyl)phosphine (3.52 mg, 10% mol), and cesium carbonate (97.7 mg, 0.3 mmol) were put in a Biotage microwave vial (size 2–5 mL) with a magnetic stirring bar. The vial was sealed and then purged with nitrogen to remove the oxygen. About 2 mL of degased toluene was added and the reaction was heated with an oil bath at 120 °C (reaction under pressure) for 24 h. Then the reaction was cooled to room temperature and the polymer was precipitated in methanol, filtered through the 0.45 μm nylon filter, and washed on Soxhlet apparatus with acetone, hexanes, and chloroform. The chloroform fraction was reduced to 20–30 mL and then precipitated in methanol, filtered through the 0.45 μm nylon filter, and air-dried to give 90 mg of the desired polymer (yield: 88%). **P4**: M_n = 42 kDa; PDI = 1.9.

*Polymer **P8** Synthesis*: 2,5-bis(4-Dodecyl-5-bromo-thien-2-yl)selenophene (0.0790 g, 0.1 mmol), 5-(9-heptadecanyl)selenopheno[3,4-*c*]pyrrole-4,6-dione (0.0439 g, 0.1 mmol), palladium (II) acetate (1.12 mg, 5% mol), pivalic acid (10.2 mg, 0.1 mmol), tris(2-methoxyphenyl)phosphine (3.52 mg, 10% mol), and cesium carbonate (97.7 mg, 0.3 mmol) were put in a Biotage microwave vial (size 2–5 mL) with a magnetic stirring bar. The vial was sealed and then purged with nitrogen to remove the oxygen. 2 mL of degased toluene was added and the reaction was heated with an oil bath at 120 °C (reaction under pressure) for 24 h. Then the reaction was cooled to room temperature and the polymer precipitated in methanol, filtered through the 0.45 μm nylon filter, and washed on Soxhlet apparatus with acetone, hexanes, and chloroform. The chloroform fraction was reduced to 20–30 mL and then precipitated in methanol, filtered through the 0.45 μm nylon filter and air-dried to give 97 mg of the desired polymer (yield: 91%). **P8**: M_n = 41 kDa; PDI = 2.1.

*Polymer **P9** Synthesis*: In a 10 mL oven-dried microwave vial, 367.2 mg (0.493 mmol) of 4,4-bis(2-ethylhexyl)-2,6-bis(trimethyltin)-dithieno[3,2-*b*:2′,3′-*d*]silole, 231.9 mg (0.493 mmol) of dibromo-5-octylseleno[3,4-*c*]pyrrole-4,6-dione, 13.5 mg (3% mol) of tris(dibenzylideneacetone) dipalladium(0) (Pd_2dba_3), and 18.1 mg (12% mol) of triphenyl arsine ($AsPh_3$) were added. The vial was purged with argon, and then 5.4 mL of degassed toluene/dimethylformamide (DMF) (10:1, v/v) was added and the resulting solution was stirred at 115 °C under argon. After 72 h of polymerization, bromobenzene (1 eq) was added to the reaction mixture and reacted for 1 h at 115 °C. Then, trimethylphenyltin (1 eq) was added to the reaction and reacted at 115 °C for an additional hour to complete the end-capping reaction. The dark blue polymerization solution was cooled to room temperature and precipitate into methanol. The polymer was collected by filtration, dried, and extracted successively with acetone, hexanes, and dichloromethane using a Soxhlet extraction apparatus. The remaining solid was extracted with chloroform. After evaporation of the chloroform under reduced pressure (10 mL) and precipitation in methanol (200 mL), **P9** was collected by filtration (206 mg, 57% yield). **P9**: M_n = 29 kDa; PDI = 1.6.

Supporting Information

Supporting Information is available from the Wiley Online Library or from the author.

Acknowledgments

This work was supported by an NSERC RDC grant and Hydro-Quebec (IREQ). The authors would also like to gratefully thank Marie Vangheluwe and Cheikhou Ba for the contribution in the *J–V* curves program.

Received: June 19, 2015
Revised: August 6, 2015
Published online:

[1] Q. Zhang, B. Kan, F. Liu, G. Long, X. Wan, X. Chen, Y. Zuo, W. Ni, H. Zhang, M. Li, Z. Hu, F. Huang, Y. Cao, Z. Liang, M. Zhang, T. P. Russell, Y. Chen, *Nat. Photon.* **2015**, *9*, 35.
[2] Y. Chen, X. Wan, G. Long, *Acc. Chem. Res.* **2013**, *46*, 2645.

[3] A. Mishra, P. Bauerle, *Angew. Chem. Int. Ed.* **2012**, *51*, 2020.
[4] P. Gautam, R. Misra, S. A. Siddiqui, G. D. Sharma, *ACS Appl. Mater. Interfaces* **2015**, *7*, 10283.
[5] P. Gautam, R. Misra, S. A. Siddiqui, G. D. Sharma, *Org. Electron.* **2015**, *9*, 76.
[6] J. You, L. Dou, K. Yoshimura, T. Kato, K. Ohya, T. Moriarty, K. Emery, C.-C. Chen, J. Gao, G. Li, Y. Yang, *Nat. Commun.* **2013**, *4*, 1446.
[7] Y. Liu, J. Zhao, Z. Li, C. Mu, W. Ma, H. Hu, K. Jiang, H. Lin, H. Ade, H. Yan, *Nat. Commun.* **2014**, *5*, 1.
[8] S.-H. Liao, H.-J. Jhuo, P.-N. Yeh, Y.-S. Cheng, Y.-L. Li, Y.-H. Lee, S. Sharma, S.-A. Chen, *Sci. Rep.* **2014**, *4*, 1.
[9] J.-D. Chen, C. Cui, Y.-Q. Li, L. Zhou, Q.-D. Ou, C. Li, J.-X. Tang, *Adv. Mater.* **2015**, *27*, 1035.
[10] C. H. Peters, I.-T. Sachs-Quintana, J. P. Kastrop, S. Beaupré, M. Leclerc, M. D. McGehee, *Adv. Energy. Mater.* **2011**, *1*, 491.
[11] J. Kong, S. Song, M. Yoo, G. Y. Lee, O. Kwon, J. K. Park, H. Back, G. Kim, S. H. Lee, H. Suh, K. Lee, *Nat. Commun.* **2014**, *5*, 1.
[12] Z. He, B. Xiao, F. Liu, H. Wu, Y. Yang, S. Xiao, C. Wang, T. P. Russell, Y. Cao, *Nat. Photon.* **2015**, *9*, 174.
[13] L. Ye, S. Q. Zhang, W. C. Zhao, H. F. Yao, J. H. Hou, *Chem. Mater.* **2014**, *26*, 3603.
[14] T. L. Nguyen, H. Choi, S. J. Ko, M. A. Uddin, B. Walker, S. Yum, J. E. Jeong, M. H. Yun, T. J. Shin, S. Hwang, J. Y. Kim, H. Y. Woo, *Energy Environ. Sci.* **2014**, *7*, 3040.
[15] H. Choi, S.-J. Ko, T. Kim, P.-O. Morin, B. Walker, B. H. Lee, M. Leclerc, J. Y. Kim, A. J. Heeger, *Adv. Mater.* **2015**, *27*, 3318.
[16] R. Po, G. Bianchi, C. Carbonera, A. Pellegrino, *Macromolecules* **2015**, *48*, 453.
[17] Y. Zou, A. Najari, P. Berrouard, S. Beaupré, B. R. Aïch, Y. Tao, M. Leclerc, *J. Am. Chem. Soc.* **2010**, *132*, 5330.
[18] C. Piliego, T. W. Holcombe, J. D. Douglas, C. H. Woo, P. M. Beaujuge, J. M. J. Fréchet, *J. Am. Chem. Soc.* **2010**, *132*, 7595.
[19] C. Cabanetos, A. El Labban, J. A. Bartelt, J. D. Douglas, W. R. Mateker, J. M. J. Fréchet, M. D. McGehee, P. M. Beaujuge, *J. Am. Chem. Soc.* **2013**, *135*, 4656.
[20] G. Zhang, Y. Fu, Q. Zhang, Z. Xie, *Chem. Commun.* **2010**, *46*, 4997.
[21] X. Guo, N. Zhou, S. J. Lou, J. Smith, D. B. Tice, J. W. Hennek, R. P. Ortiz, J. L. T. Navarette, S. Li, J. Strzalka, L. X. Chen, R. P. H. Chang, A. Facchetti, T. J. Marks, *Nat. Photon.* **2013**, *7*, 825.
[22] J. Jo, A. Prón, P. Berrouard, W. L. Leong, J. D. Yuen, J. S. Moon, M. Leclerc, A. J. Heeger, *Adv. Energy Mater.* **2012**, *2*, 1397.
[23] X. Guo, A. Faccetti, T. J. Marks, *Chem. Rev.* **2014**, *114*, 8943.
[24] S. Beaupré, A. Prón, S. H. Drouin, A. Najari, L. G. Mercier, A. Robitaille, M. Leclerc, *Macromolecules* **2012**, *45*, 6906.
[25] Z. He, C. Zhong, S. Su, M. Xu, H. Wu, Y. Cao, *Nat. Photon.* **2012**, *6*, 591.
[26] H. P. Kim, S. J. Lee, A. B. Mohd Yusoff, J. Jang, *IEEE. J. Photovolt.* **2015**, *5*, 897.
[27] M. Jeffries-EL, B. M. Kobilka, B. J. Hale, *Macromolecules* **2014**, *47*, 7253.
[28] D. H. Wang, P.-O. Morin, C.-L. Lee, A. K. K. Kyaw, M. Leclerc, A. J. Heeger, *J. Mater. Chem. A.* **2014**, *2*, 15052.
[29] W. Li, Y. Zhou, B. V. Andersson, L. M. Andersson, Y. Thomann, C. Veit, K. Tvingstedt, R. Qin, Z. Bo, O. Inganäs, U. Würfel, F. Zhang, *Org. Electron.* **2011**, *12*, 1544.
[30] D. Di Nuzzo, A. Aguirre, M. Shahid, V. S. Gevaerts, S. C. J. Meskers, R. A. J. Janssen, *Adv. Mater.* **2010**, *22*, 4321.
[31] T. Salim, L. H. Wong, B. Brauer, R. Kukreja, Y. L. Foo, Z. Bao, Y. M. Lam, *J. Mater. Chem.* **2011**, *21*, 242.
[32] J. C. Wang, X. C. Ren, S. Q. Shi, C. W. Leung, P. K. L. Chan, *Org. Electron.* **2011**, *12*, 880.
[33] B. R. Aïch, S. Beaupré, M. Leclerc, Y. Tao, *Org. Electron.* **2014**, *15*, 543.
[34] B. R. Aïch, J. Lu, S. Beaupré, M. Leclerc, Y. Tao, *Org. Electron.* **2013**, *12*, 1736.
[35] D. H. Wang, A. Prón, M. Leclerc, A. J. Heeger, *Adv. Funct. Mater.* **2013**, *23*, 1297.
[36] T.-Y. Chu, S-W. Tsang, J. Zhou, P. G. Verly, J. Lu, S. Beaupré, M. Leclerc, Y. Tao, *Sol. Energy Mater. Sol. Cells.* **2012**, *96*, 155.
[37] T.-Y. Chu, J. Lu, S. Beaupré, Y. Zhang, J.-R. Pouliot, S. Wakim, J. Zhou, M. Leclerc, Z. Li, J. Ding, Y. Tao, *J. Am. Chem. Soc.* **2011**, *133*, 4250.
[38] S.-W. Chang, H. Waters, J. Kettle, Z.-R. Kuo, C.-H. Li, C.-Y. Yu, M. Horie, *Macromol. Rapid Commun.* **2012**, *33*, 1927.
[39] E. Iizuka, M. Wakioka, F. Ozawa, *Macromolecules* **2015**, *48*, 2989.
[40] T.-Y. Chu, J. Lu, S. Beaupré, Y. Zhang, J.-R. Pouliot, J. Zhou, A. Najari, M. Leclerc, Y. Tao, *Adv. Funct. Mater.* **2012**, *22*, 2345.
[41] B. C. Thompson, Y.-G. Kim, J. R. Reynolds, *Macromolecules* **2005**, *385*359.
[42] Y. Sun, J. H. Seo, C. J. Takacs, J. Seifter, A. J. Heeger, *Adv. Mater.* **2011**, *23*, 1679.
[43] M. P. Ouattara, S. Lenfant, D. Vuillaume, M. Pézolet, J.-F. Rioux-Dubé, J. Brisson, M. Leclerc, *Macromolecules* **2013**, *46*, 6408.